Rapid Communications

Topology-optimized dual-polarization Dirac cones

Zin Lin,[1] Lysander Christakis,[2] Yang Li,[1] Eric Mazur,[1] Alejandro W. Rodriguez,[3] and Marko Lončar[1,*]
[1]*John A. Paulson School of Engineering and Applied Sciences, Harvard University, Cambridge, Massachusetts 02138, USA*
[2]*Department of Physics, Yale University, New Haven, Connecticut 06511, USA*
[3]*Department of Electrical Engineering, Princeton University, Princeton, New Jersey 08544, USA*

(Received 29 May 2017; revised manuscript received 28 January 2018; published 23 February 2018)

We apply a large-scale computational technique, known as topology optimization, to the inverse design of photonic Dirac cones. In particular, we report on a variety of photonic crystal geometries, realizable in simple isotropic dielectric materials, which exhibit dual-polarization Dirac cones. We present photonic crystals of different symmetry types, such as fourfold and sixfold rotational symmetries, with Dirac cones at different points within the Brillouin zone. The demonstrated and related optimization techniques open avenues to band-structure engineering and manipulating the propagation of light in periodic media, with possible applications to exotic optical phenomena such as effective zero-index media and topological photonics.

DOI: 10.1103/PhysRevB.97.081408

Introduction. Dirac cones (DCs), or conical dispersions [1,2], have received broad attention due to their special properties affecting light transport in photonic systems, such as effective zero-index behavior [1,3–11], exceptional points [12,13], photonic *Zitterbewegung* [14], and topologically protected states [15,16]. So far, DCs have been primarily studied in simple geometries based on circular pillars or air holes on a periodic lattice [1,3,5,7,9,10]. One exception is our previous work [13], which exploited topology optimization (TO) techniques to demonstrate higher-order DCs (precursors to exceptional points [12,13]) in complex structures. TO, which was first proposed more than a decade ago [17], employs gradient-based algorithms to efficiently handle a very large design space, considering every pixel or voxel as a degree of freedom in an extensive two-dimensional (2D) or three-dimensional (3D) computational domain [18–21]. Recently, inverse-designed materials based on TO have been utilized to improve the performance of optical devices such as mode splitters, demultiplexers, and wavelength converters [18,22–26].

Here, we apply TO toward the design of unprecedented dispersion features in photonic crystals (PhCs), namely, two overlapping DCs with dual polarizations (DPDC): one having transverse magnetic polarization ($\mathbf{H}\cdot\hat{\mathbf{z}}=0$) and the other having transverse electric polarization ($\mathbf{E}\cdot\hat{\mathbf{z}}=0$). We show that if such overlapping dispersions are designed at the Γ point of the Brillouin zone of a square-lattice PhC, two Dirac-like cones form, each from the degeneracy of three linear bands and with a corresponding Berry phase of zero [2]. As a consequence of the DPDC at the Γ point, these PhCs exhibit zero-index behavior regardless of the polarization of the incident light. Furthermore, we also demonstrate DPDCs formed by the overlap of two true Dirac cones, each consisting of two linear bands and with a nontrivial Berry phase [2], at the **K** point of a hexagonal PhC. This type of DPDC has implications for all-dielectric topological photonics [16,27].

Recent years have witnessed an exciting quest for exotic composite materials along with unusual states of matter involving enhanced optical, mechanical, and quantum properties [28–31]. However, there has been comparatively less effort devoted to discovering unconventional structures that can enhance the functionality of ordinary materials, such as ubiquitous low-loss isotropic dielectrics. Our work represents an effort to leverage the capabilities of established but underutilized inverse design tools to uncover increased functionalities for simple dielectrics.

Dual-polarization Dirac cones. Power emitted by a time-harmonic current source $\mathbf{J}\sim e^{i\omega t}$, proportional to the local density of states (LDOS), offers a convenient optimization framework for designing eigenmodes at a given frequency ω. This follows the well-known principle that emitted power, $f(\mathbf{E},\mathbf{J},\omega;\epsilon)=-\mathrm{Re}[\int \mathbf{J}^*\cdot\mathbf{E}d\mathbf{r}]$, is maximized when the source couples to a long-lived resonance [22]. Here, the electric field **E** is simply the solution of the steady-state Maxwell equation, $\nabla\times\frac{1}{\mu}\nabla\times\mathbf{E}-\omega^2\epsilon(\mathbf{r})\mathbf{E}=i\omega\mathbf{J}$. The goal of TO is to discover the dielectric profile $\epsilon(\mathbf{r})$ that maximizes f for any given **J** and ω. In what follows, we judiciously choose $\mathbf{J}(\mathbf{r})$ and the symmetries of the unit cell to construct PhCs with a variety of intriguing spectral features (see Supplemental Material for details [32]). In particular, we apply TO to design *six accidentally degenerate* modes of monopolar (M), dipolar (D), and quadrupolar (Q) profiles (inset of Fig. 1) that transform according to the A and E irreducible representations of the C_{4v} point group, and which, in turn, give rise to conical dispersions in the vicinity of their degeneracy [2,33,34]. We emphasize that designing such a *sixfold* degeneracy poses a significant challenge for conventional design and even for sophisticated, heuristic optimization algorithms such as particle swarms, simulated annealing, or genetic algorithms [35–37], but can be susceptible to efficient gradient-based TO techniques, in combination with a proper problem formulation.

Figure 1 shows a topology-optimized PhC unit cell and its associated band structure, which exhibits two overlapping DCs at the Γ point; one with transverse electric (TE) and

*loncar@seas.harvard.edu

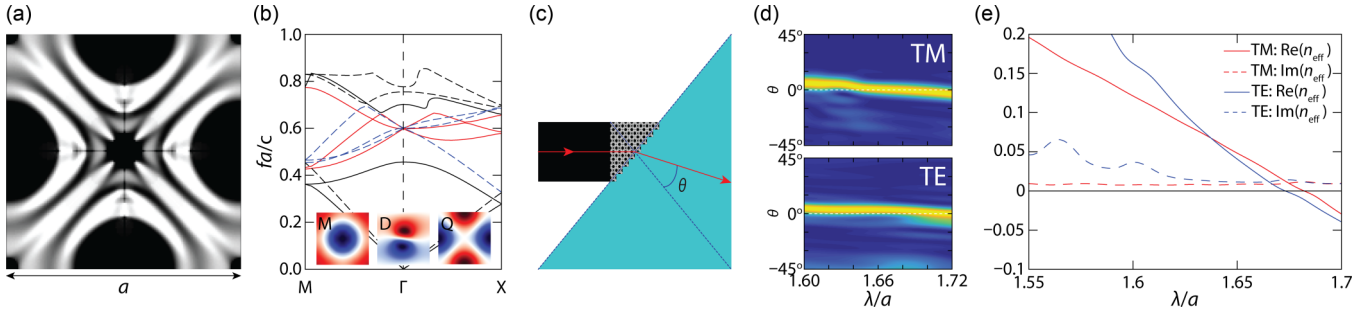

FIG. 1. (a) Topology-optimized unit cell. Black (white) regions have relative permittivity $\epsilon_r \approx 5.5$ ($\epsilon_r = 1$). Gray regions with intermediate permittivities are also seen. Note that the structure obeys C_{4v} symmetry. (b) The band structure reveals two overlapping Dirac cones, one for TM polarization (solid lines) and the other for TE polarization (dashed lines). Transverse magnetic Dirac bands (dark red lines) are formed by the degeneracy of one monopolar (M) and two dipolar (D) modes manifested by the E_z component, whereas transverse electric Dirac bands (light-blue lines) are formed by the degeneracy of two dipolar (D) modes and one quadrupolar (Q) mode manifested by the H_z component (see figure inset). (c) Configuration of the prism test designed to illustrate effective zero-index behavior for designs with dual-polarization Dirac cones (DPDCs). (d) FDTD analysis of the DPDC structures and their far-field patterns through the prism test show orthogonally emerging beams at the prism facet ($\theta = 0$), validating the effective zero-index behavior for both TM- and TE-polarized waves incident on the nonbinary design. Also shown are the retrieved TM and TE effective indices for the nonbinary design (e).

the other with transverse magnetic (TM) polarization. Note that the DC in our design is the so-called generalized DC typically characterized by the presence of an extra flatband [2,38]. Within the DPDC, TM Dirac bands are formed by the degeneracy of one monopolar (M) and two dipolar (D) modes, whereas TE Dirac bands are formed by the degeneracy of two dipolar (D) modes and one quadrupolar (Q) mode. The optimized structure consists of high dielectric regions ($\epsilon_r = 5.5$), typical of common materials such as silicon nitride or titania, in a background of air ($\epsilon_r = 1$). Intermediate permittivities, $\epsilon_r \in (1,5.5)$, are also seen as a result of fine-tuning the necessary modal frequencies to ensure a perfect overlap. The resulting *gray-scale* PhC has altogether *six* DPDC modes whose frequencies are degenerate to within 0.1%, an accuracy limited only by numerical resolution [39,40]. Here, we note that in a few initial rounds of optimization, we deliberately optimize for a TM quadrupole at $f_{TMQ} \sim 0.75\, f_D$ and a TE monopole at $f_{TEM} \sim 1.25\, f_D$ *in addition* to the six degenerate modes forming the DC. We find that such a procedure for "mode separation" helps ensure well-isolated conical dispersions.

DCs at the center of the Brillouin zone correspond to zero-index behavior when the appropriate homogenization criteria are met [1,5,41–43] (see Supplemental Material for details [32]). We perform full-wave finite-difference time domain (FDTD) analysis on our DPDC structures and show that they indeed exhibit various zero-index characteristics. One characteristic of a zero-index medium (ZIM) is observed in the so-called "prism" test [5], where plane waves normally incident on a facet of a zero-index prism emerge at a right angle from another facet. Alternatively, one can also simulate the complex transmission and reflection coefficients of the ZIM, from which effective constitutive parameters can be extracted [1,5]. As shown in Fig. 1(c), we perform a prism test by illuminating one side of a 45°-45°-90° triangular region made up of DPDC unit cells and then measuring the far-field patterns emerging out of the diagonal (hypotenuse) facet. Note that θ is the refraction angle between the direction of the emerging beam and the facet normal. Figure 1(d) shows smooth Gaussian beam profiles in the far field with the refraction angles crossing zero around the Dirac-cone wavelengths for both TE and TM polarizations. Index retrievals [Fig. 1(e)] also confirm the zero-index behavior with the effective index crossing $n = 0$ around $1.675\lambda/a$. It must be noted that in our structures, zero-index behavior is only observed for normal incidence; illumination at oblique incident angles excite modes which do not exhibit zero-index behavior, as is the case for most Dirac-cone ZIM [44].

While Fig. 1 demonstrates a perfect DPDC, the gray-scale dielectric profile poses a significant fabrication challenge (although it may be implemented in the radio frequency regime). Here, we examine a binary regularized version better suited for experimental realization. The modified structure [Fig. 2(a)] is obtained via two stages: first, we apply threshold projection filters [45] *during* the optimization process to produce a binary design; then, we feed the intermediate binary design into a *post*-optimization pixel-averaging routine to weed out the fine features and regularize the structure (see also the Supplemental Material for details [32]). The associated band structure [Fig. 2(b)] shows a DPDC albeit with a *spoiled* overlap due to a small frequency gap of ~1% between the TE and TM DCs. Figures 2(c) and 2(d) show the corresponding prism tests and index retrieval analyses. Arguably, the optimally fine-tuned gray-scale structure shows better performance than the completely binary version. This is due to the following reasons: for the gray-scale version, the zero-index crossing is perfectly linear and virtually degenerate for both polarizations; for the binary version, the crossings are separated by about 1% and the part of the effective index shows a constant zero value while the imaginary part depicts a bump around the zero crossing, which corresponds to a small band gap near the Dirac-point frequency [5]. Nevertheless, the modified structures clearly feature a range of wavelengths where *near-zero-index* behavior is observed for both polarizations, which make them realistic candidates for practical applications. We note that an approach to realize DPDCs and polarization-independent zero-index behavior was recently proposed [46], which necessitates the use of complex metacrystals based on patterning an anisotropic

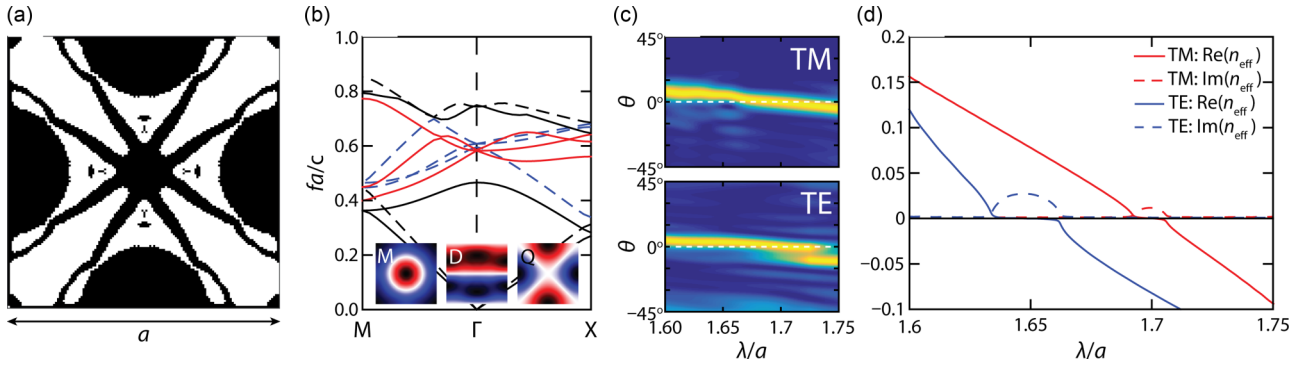

FIG. 2. (a) Binary regularized version of a DPDC PhC unit cell, with the corresponding band structure (b) showing TM (solid lines) and TE (dashed lines) Dirac cones. (c) FDTD analysis and the far-field patterns through the prism test show orthogonally emerging beams at the prism facet ($\theta = 0$), validating the effective zero-index behavior for both TM- and TE-polarized incident waves. (d) Also shown are the TM and TE effective indices retrieved from scattering coefficients.

elliptic metamaterial. In contrast, we identify DPDCs by virtue of unconventional geometries that can be imprinted on simple ordinary isotropic dielectrics. Another design of DPDCs is based on a 3D simple cubic array of core-shell structures [47], making it infeasible for fabrication using a standard planar process. In contrast, our design is essentially 2D and can be fabricated by patterning a film on a substrate.

The appearance of complicated features in the DPDC geometry (Fig. 1) can be attributed to numerous stringent conditions imposed upon the optimization process. As noted above, one such condition is the mode separation constraint which pushes certain extraneous modes away from the Dirac degeneracy. We find that relaxing this constraint leads to a simple DPDC structure with regular geometric features [Fig. 3(a)] although the proximity of an unintentional TM quadrupole mode in the band structure engenders an anticrossing (aka mode mixing [48]) off the Γ point near the Dirac frequency [Fig. 3(b)]. Nevertheless, FDTD analyses of Fig. 3(a) clearly show that, for both TE and TM polarizations, the refracted beams cross zero degrees around the Dirac-point wavelength [Fig. 3(c)]. The corresponding effective indices show near-zero behavior around the Dirac-point wavelength [Fig. 3(d)]. Compared with the design in Fig. 2(a), the "four-hole" structure [Fig. 3(a)] has a much simpler geometry, making the practical fabrication significantly easier. Furthermore, the dielectric medium of the four-hole structure has a relative permittivity $\epsilon = 3.3$, which can be realized by polymers, such as polyferrocene [49], in the optical regime.

Dirac cones at the **K** *point.* To demonstrate the versatility of our approach, we proceed to design DPDCs based on a hexagonal lattice with symmetry properties distinct from those found on a square lattice. In particular, we focus on the **K** point of the Brillouin zone, where two dipolar eigenmodes that transform according to the E irreducible representations of the C_{3v} point group form a *deterministic* DC, i.e, a DC that arises as a consequence of the symmetry of the lattice [2,33]. We show that we can overlap two such DCs, one with TM polarization and the other with TE polarization, thus restoring electromagnetic duality [16] in the vicinity of the fourfold degenerate Dirac point. Specifically, we employ the LDOS TO formulation to design degenerate TM and TE dipolar modes while imposing C_{3v} symmetry via suitable transformations which ensure the concurrence of the corresponding degenerate partner for each polarization, leading to DPDCs.

Figure 4 shows complex geometries discovered by TO and the corresponding band structure with overlaid TE and TM DCs at **K** point. The gap between the two Dirac points is as small as <0.1%, only limited by numerical discretization

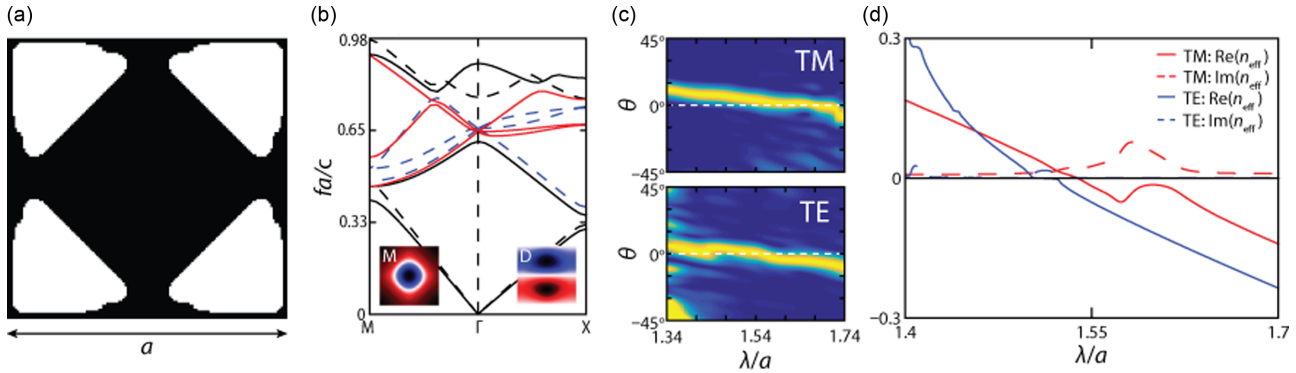

FIG. 3. (a) Binary regularized DPDC PhC with fabrication-friendly features. (b) The corresponding band structure shows two overlapping TM (solid lines) and TE (dashed lines) Dirac cones. (c) FDTD analysis and the far-field patterns through the prism test [Fig. 1(c)] show orthogonally emerging beams at the prism facet ($\theta = 0$), validating the effective zero index behavior for both TM- and TE-polarized incident waves. (d) Also shown are the TM and TE retrieved effective indices.

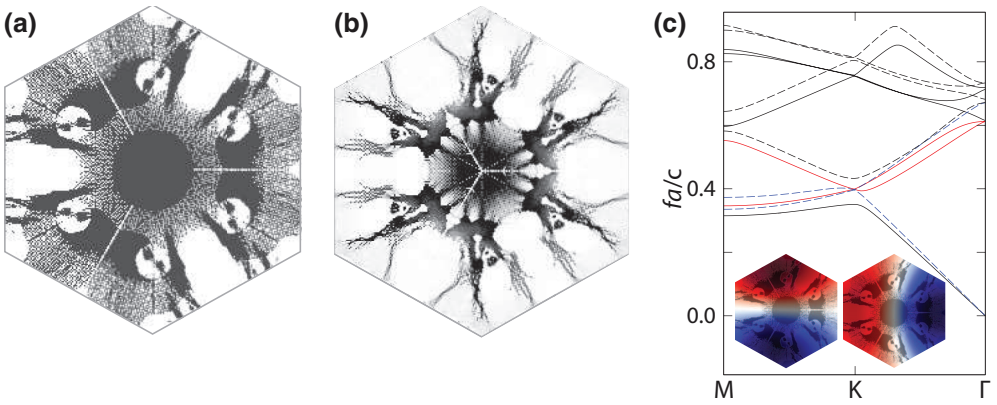

FIG. 4. Detailed image of a (a) low-index ($\epsilon_r = 3.3$) and a (b) high-index ($\epsilon_r = 9$) topology-optimized hexagonal unit cell. (c) Band structure of the low-index design exhibiting overlaid TE (dashed line) and TM (solid lines) Dirac bands (red and blue). The degenerate modes (insets) transform according to the E irreducible representation of the C_{3v} group.

errors. This structure is a proof-of-principle 2D design, based on ordinary isotropic dielectric materials, that hosts overlaid TE/TM DCs at a non-Γ point of a PhC. Moreover, this structure stands in contrast to more sophisticated recent designs using 2D metacrystals [16] or 3D hexagonal PhCs [27]. Since DPDCs at the **K** point of a hexagonal lattice are important precursors to nontrivial topological states [15,16,27], our method suggests an alternative precursor from which one may realize a so-called photonic topological insulator (PTI). Since our focus here is realizing DPDCs, we will not pursue making a PTI here. However, it is worth mentioning that there are well-known techniques to introduce nontrivial topological band gaps into DPDCs based on suitable bianisotropic perturbations, such as by introducing off-axis propagation ($k_z \neq 0$), by systematic reduction of mirror symmetry, or by modifications that mix TE and TM polarizations while preserving the pseudospin distinction [16]. Although the TO-discovered geometry might be quite challenging to fabricate due to the existence of pixel-thin hairy features, we note that these features do not indicate a fundamental limitation of our technique but are an artifact of underlying image-transformation steps which impose undue constraints on the optimization process. In the Supplemental Material, we discuss such drawbacks as well as possible ways to mitigate them.

Conclusion and remarks. While some of the optimized designs we have presented might prove challenging, although not impossible, to fabricate at visible or near-infrared frequencies, they can be readily realized at mid- to far-IR as well as microwave frequencies via existing technologies such as computerized machining, 3D printing, laser cutting, additive manufacturing, or two-photon lithography, self-assembly of DNA molecules [50–53]. Furthermore, thin isolated features which typically beset topology-optimized designs can be removed by a variety of advanced regularization and averaging techniques [18]. The appearance of such features indicates an optimization process that is severely constrained by the design requirements of realizing TE and TM modes with the same modal profile at the same frequency. The fundamental issue underlying such a design is that in a generic structured isotropic 2D medium, TM bands tend to be at lower frequencies than TE bands, breaking the so-called electromagnetic duality. While we have shown that our TO formulation is capable of restoring this duality and finding DPDCs on a 2D lattice, this comes at the expense of a highly irregular structure which needs to be fine-tuned with thin sensitive features. In contrast, we surmise that three-dimensional platforms will offer even greater flexibility. For example, it is known that TM modes tend to experience effectively different index of refraction relative to TE modes in 3D PhC slabs, e.g., depending on whether the PhC geometry consists of holes or pillars [48].

In future work, we will consider optimization in full 3D multilayered geometries, which we expect will open up even more exciting opportunities for new structural designs in the fields of metasurfaces, metamaterials, and topological photonics.

Acknowledgments. The authors thank P. Camayd-Muñoz and O. Reshef for discussions. This work was partially supported by the Air Force Office of Scientific Research under Contract No. FA9550-14-1-0389, by the National Science Foundation under Grants No. DMR-1454836 and No. DMR-1360889, and by the Princeton Center for Complex Materials, a MRSEC supported by NSF Grant No. DMR-1420541. Z.L. is supported by the National Science Foundation Graduate Research Fellowship Program under Grant No. DGE1144152.

Z.L., L.C., and Y.L. contributed equally to this work.

[1] X. Huang, Y. Lai, Z. H. Hang, H. Zheng, and C. T. Chan, Nat. Mater. **10**, 582 (2011).

[2] J. Mei, Y. Wu, C. T. Chan, and Z.-Q. Zhang, Phys. Rev. B **86**, 035141 (2012).

[3] P. Moitra, Y. Yang, Z. Anderson, I. I. Kravchenko, D. P. Briggs, and J. Valentine, Nat. Photonics **7**, 791 (2013).

[4] H. Suchowski, K. O'Brien, Z. J. Wong, A. Salandrino, X. Yin, and X. Zhang, Science **342**, 1223 (2013).

[5] Y. Li, S. Kita, P. Camayd-Muñoz, O. Reshef, D. I. Vulis, M. Yin, M. Lončar, and E. Mazur, Nat. Photonics **9**, 738 (2015).

[6] H. Hajian, E. Ozbay, and H. Caglayan, Appl. Phys. Lett. **109**, 031105 (2016).

[7] X.-T. He, Z.-Z. Huang, M.-L. Chang, S.-Z. Xu, F.-L. Zhao, S.-Z. Deng, J.-C. She, and J.-W. Dong, ACS Photonics **3**, 2262 (2016).

[8] I. Liberal and N. Engheta, Nat. Photonics **11**, 149 (2017).

[9] S. Kita, Y. Li, P. Camayd-Muñoz, O. Reshef, D. I. Vulis, R. W. Day, E. Mazur, and M. Lončar, Opt. Express **25**, 8326 (2017).

[10] D. I. Vulis, Y. Li, O. Reshef, P. Camayd-Muñoz, M. Yin, S. Kita, M. Lončar, and E. Mazur, Opt. Express **25**, 12381 (2017).

[11] O. Reshef, P. Camayd-Muñoz, D. I. Vulis, Y. Li, M. Lončar, and E. Mazur, ACS Photonics **4**, 2385 (2017).

[12] B. Zhen, C. W. Hsu, Y. Igarashi, L. Lu, I. Kaminer, A. Pick, S.-L. Chua, J. D. Joannopoulos, and M. Soljačić, Nature (London) **525**, 354 (2015).

[13] Z. Lin, A. Pick, M. Lončar, and A. W. Rodriguez, Phys. Rev. Lett. **117**, 107402 (2016).

[14] X. Zhang, Phys. Rev. Lett. **100**, 113903 (2008).

[15] L. Lu, J. D. Joannopoulos, and M. Soljačić, Nat. Photonics **8**, 821 (2014).

[16] A. B. Khanikaev, S. H. Mousavi, W.-K. Tse, M. Kargarian, A. H. MacDonald, and G. Shvets, Nat. Mater. **12**, 233 (2013).

[17] O. Sigmund and J. S. Jensen, Philos. Trans. R. Soc. London A **361**, 1001 (2003).

[18] J. Jensen and O. Sigmund, Laser Photonics Rev. **5**, 308 (2011).

[19] K. Svanberg, SIAM J. Optim. **12**, 555 (2002).

[20] J.-F. Bonnans, J. C. Gilbert, C. Lemaréchal, and C. A. Sagastizábal, *Numerical Optimization: Theoretical and Practical Aspects* (Springer Science & Business Media, Berlin, 2006).

[21] S. G. Johnson, The NLopt nonlinear-optimization package, http://ab-initio.mit.edu/nlopt

[22] X. Liang and S. G. Johnson, Opt. Express **21**, 30812 (2013).

[23] A. Y. Piggott, J. Lu, K. G. Lagoudakis, J. Petykiewicz, T. M. Babinec, and J. Vučković, Nat. Photonics **9**, 374 (2015).

[24] J. Lu and J. Vučković, Opt. Express **21**, 13351 (2013).

[25] B. Shen, P. Wang, R. Polson, and R. Menon, Nat. Photonics **9**, 378 (2015).

[26] Z. Lin, X. Liang, M. Lončar, S. G. Johnson, and A. W. Rodriguez, Optica **3**, 233 (2016).

[27] A. Slobozhanyuk, S. H. Mousavi, X. Ni, D. Smirnova, Y. S. Kivshar, and A. B. Khanikaev, Nat. Photonics **11**, 130 (2017).

[28] Q. Wang, J. A. Jackson, Q. Ge, J. B. Hopkins, C. M. Spadaccini, and N. X. Fang, Phys. Rev. Lett. **117**, 175901 (2016).

[29] A. Drozdov, M. Eremets, I. Troyan, V. Ksenofontov, and S. Shylin, Nature (London) **525**, 73 (2015).

[30] Z. Qin, G. S. Jung, M. J. Kang, and M. J. Buehler, Sci. Adv. **3**, e1601536 (2017).

[31] Z. J. Wong, Y.-L. Xu, J. Kim, K. O'Brien, Y. Wang, L. Feng, and X. Zhang, Nat. Photonics **10**, 796 (2016).

[32] See Supplemental Material at http://link.aps.org/supplemental/10.1103/PhysRevB.97.081408 for details on the topology optimization procedure, homogenization criteria for zero-index media, and other details for the design of the structures shown in this Rapid Communication.

[33] K. Sakoda, J. Opt. Soc. Am. B **29**, 2770 (2012).

[34] K. Sakoda, Opt. Express **20**, 25181 (2012).

[35] S. Kirkpatrick, J. Stat. Phys. **34**, 975 (1984).

[36] D. E. Goldberg and J. H. Holland, Mach. Learn. **3**, 95 (1988).

[37] J. Kennedy, in *Encyclopedia of Machine Learning* (Springer, New York, 2011), pp. 760–766.

[38] B. Dóra, J. Kailasvuori, and R. Moessner, Phys. Rev. B **84**, 195422 (2011).

[39] J.-M. Jin, *The Finite Element Method in Electromagnetics* (Wiley, New York, 2014).

[40] C. Geuzaine and J.-F. Remacle, Int. J. Nume. Methods Eng. **79**, 1309 (2009).

[41] C. R. Simovski and S. A. Tretyakov, Phys. Rev. B **75**, 195111 (2007).

[42] R. A. Shore and A. D. Yaghjian, Radio Sci. **42**, RS6S21 (2007).

[43] A. Alù, A. D. Yaghjian, R. A. Shore, and M. G. Silveirinha, Phys. Rev. B **84**, 054305 (2011).

[44] P. Zhang, C. Fietz, P. Tassin, T. Koschny, and C. M. Soukoulis, Opt. Express **23**, 10444 (2015).

[45] F. Wang, B. S. Lazarov, and O. Sigmund, Struct. Multidiscip. Optim. **43**, 767 (2011).

[46] J.-R. Wang, X.-D. Chen, F.-L. Zhao, and J.-W. Dong, Sci. Rep. **6**, 22739 (2016).

[47] C.-T. Chan, X. Huang, F. Liu, and Z. H. Hang, Prog. Electromagn. Res. B **44**, 163 (2012).

[48] J. D. Joannopoulos, S. G. Johnson, J. N. Winn, and R. D. Meade, *Photonic Crystals: Molding the Flow of Light* (Princeton University Press, Princeton, NJ, 2011).

[49] T. Higashihara and M. Ueda, Macromolecules **48**, 1915 (2015).

[50] R. Borisov, G. Dorojkina, N. Koroteev, V. Kozenkov, S. Magnitskii, D. Malakhov, A. Tarasishin, and A. Zheltikov, Appl. Phys. B **67**, 765 (1998).

[51] A. Clausen, F. Wang, J. S. Jensen, O. Sigmund, and J. A. Lewis, Adv. Mater. **27**, 5523 (2015).

[52] C. Pouya, J. T. B. Overvelde, M. Kolle, J. Aizenberg, K. Bertoldi, J. C. Weaver, and P. Vukusic, Adv. Opt. Mater. **4**, 99 (2016).

[53] P. W. K. Rothemund, Nature (London) **440**, 297 (2006).